Electronic Supplementary Information

Tunable-Wavelength Nanosecond Laser Tailoring of Plasmon Resonance Spectra of Gold Nanoparticle Colloids

Thanyada Sukmanee,[a,†] Michał Szuster,[a,†] Aleksander Gorski,[a] Marcin Hołdyński,[a] Sylwester Gawinkowski[a,*]

[a] Institute of Physical Chemistry, Polish Academy of Sciences, Kasprzaka 44/52, 01-224 Warsaw, Poland.

* e-mail: sgawinkowski@ichf.edu.pl

S1. Experimental details

S1.1. Materials and chemicals

Hexadecyltrimethylammonium bromide (CTAB, ≥96.0% (AT)), gold (III) chloride solution (HAuCl4, 30 wt.% in dilute HCl, sodium borohydride (NaBH4, ≥98.0%), silver nitrate (AgNO3, ≥99.0%), and L-ascorbic acid (99%) were purchased from Sigma–Aldrich. Hydrochloric acid (HCl, 35–38% LR grade) was purchased from POCH chemicals. Nitric acid (HNO3, 65%) and acetone (99.8%) were purchased from Chempur and Linegal Chemicals, respectively. All chemicals were used without further purification. Solutions were prepared with deionized water (18.1 MΩ).

S1.2. Preparation of GNR colloids

The colloidal gold nanorods (GNRs) were synthesized using the procedures described in previous literature [1]. The seed solution was initially prepared by mixing CTAB solution (5.0 mL, 0.20 M) with $HAuCl_4$ (5.0 mL, 0.50 mM). Next, 0.60 mL of ice-cold 0.010 M $NaBH_4$ solution was added to the stirred mixture, forming a brownish-yellow solution. The seed solution was then vigorously stirred for 2 minutes and kept at 25 °C. The growth solution of GNRs was prepared by mixing 5.0 mL of CTAB solution (0.20 M) with 3 mL of $AgNO_3$ solution (4.0 mM) at 25 °C. Next, 5.0 mL of 1.0 mM $HAuCl_4$ was added to the mixture. Then, 70 µL of 0.079 M ascorbic acid solution was gently added to the mixture, causing the growth solution to change from dark yellow to colourless. Finally, 12 µL of the seed solution was added to the growth solution at 27–30 °C. The final mixture was stirred vigorously and continuously for at least 20 minutes at 27–30 °C.

S1.3. Irradiation procedure

An Opotek Radiant SE 355 LD nanosecond pulse laser, tunable from 210 nm to 2500 nm, was used to irradiate the colloidal samples. The laser repetition rate was 10 Hz, and the pulse energy was 1.0 ± 0.1 mJ. Each pulse had a length of 5 ns and the beam had a Gaussian profile with a diameter of 7 mm on the sample, resulting in a fluence of 0.65 mJ/cm^2. The irradiation of the colloidal GNR samples was carried out in a quartz cuvette (Hellma QS 100-10-40, 10 mm optical path), and the volume of the solution was 2.5 ml. The solution was continuously stirred during irradiation using a home-built magnetic stirrer at a speed of 400 rpm. All parameters

were kept constant throughout the irradiation procedure, except for the laser wavelength, which was gradually changed after each irradiation.

Initially, we estimated the pulse energy, which causes mild changes in the spectrum. First, 100 uJ pulses and the 5 minutes irradiation steps were used. The extinction measurements followed each irradiation to monitor the changes in the spectra. Those steps were repeated with increasing pulse energy by 100 uJ until small spectral changes were detected. This way, the minimum pulse energy of 800–900 uJ necessary to induce minor changes in the spectra after 5-minute irradiation was found. Using 1 mJ pulses makes the changes more prominent but not dramatic. In the second step, we used these 1 mJ pulses and irradiated the sample repeatedly with 5 minutes periods monitoring the spectra after each irradiation. That was repeated until no further changes were observed on the spectrum. This way, we found that about 25 minutes is a necessary minimum. We added another 5 minutes and used 30 min sessions at each wavelength irradiation in the following experiments.

S1.4. SEM characterization

The Nova NanoSEM 450 scanning electron microscope (SEM) was used to monitor changes in the shape and size of the GNRs. To prepare the sample substrate for SEM measurement, small pieces of a silicon wafer (0.5×0.5 cm^2) were soaked in a mixture of HCl and HNO_3 with a volume ratio of 3:1 for 24 hours to remove any organic contamination. The substrates were then rinsed with deionized water and dried at room temperature. They were mounted on SEM specimen stubs with copper. For each sample, SEM images containing at least a few hundred objects were taken.

S1.5. Image analysis

The analysis of the SEM images was conducted using numerical methods. A Python script was developed to extract information on the shapes and sizes of the registered nanoobjects from the images. The collected data was then used as input for spectral simulations. The assumption was made in this study that the shape of the nanorods could be approximated as an ellipse in order to capture and track changes in their dimensions. This approximation allowed us to estimate the longitudinal and transverse dimensions of the nanorods as the major and minor axes of ellipses, respectively. We utilized a combination of max entropy binarization and mean adaptive threshold binarization to extract the data. The entire program for the data extraction functions was as follows:

• opening the photo,

• denoising with a non-local means algorithm,

• creating a mask for distinguishing nanoparticles from the background with max entropy binarization,

• erosion and dilation of the picture to erase single points,

• creating an intermediate picture as a mask · primary picture + (1 – mask) · averaging over grayscale of primary picture,

• binarization of the picture with an adaptive mean threshold algorithm,

• approximating objects on the picture with ellipses and extracting data describing the major and minor axes of the nanorods in pixels,

• rescaling the minor and major axis dimensions from pixels to nanometers with a linear relationship between length and magnitude.

The algorithm was capable of distinguishing single nanorods from aggregate nanorods, as shown in Fig. S1. Nevertheless, objects with an area below 200 nm^2 were excluded from this analysis, as they could be artifacts resulting from the binarization step.

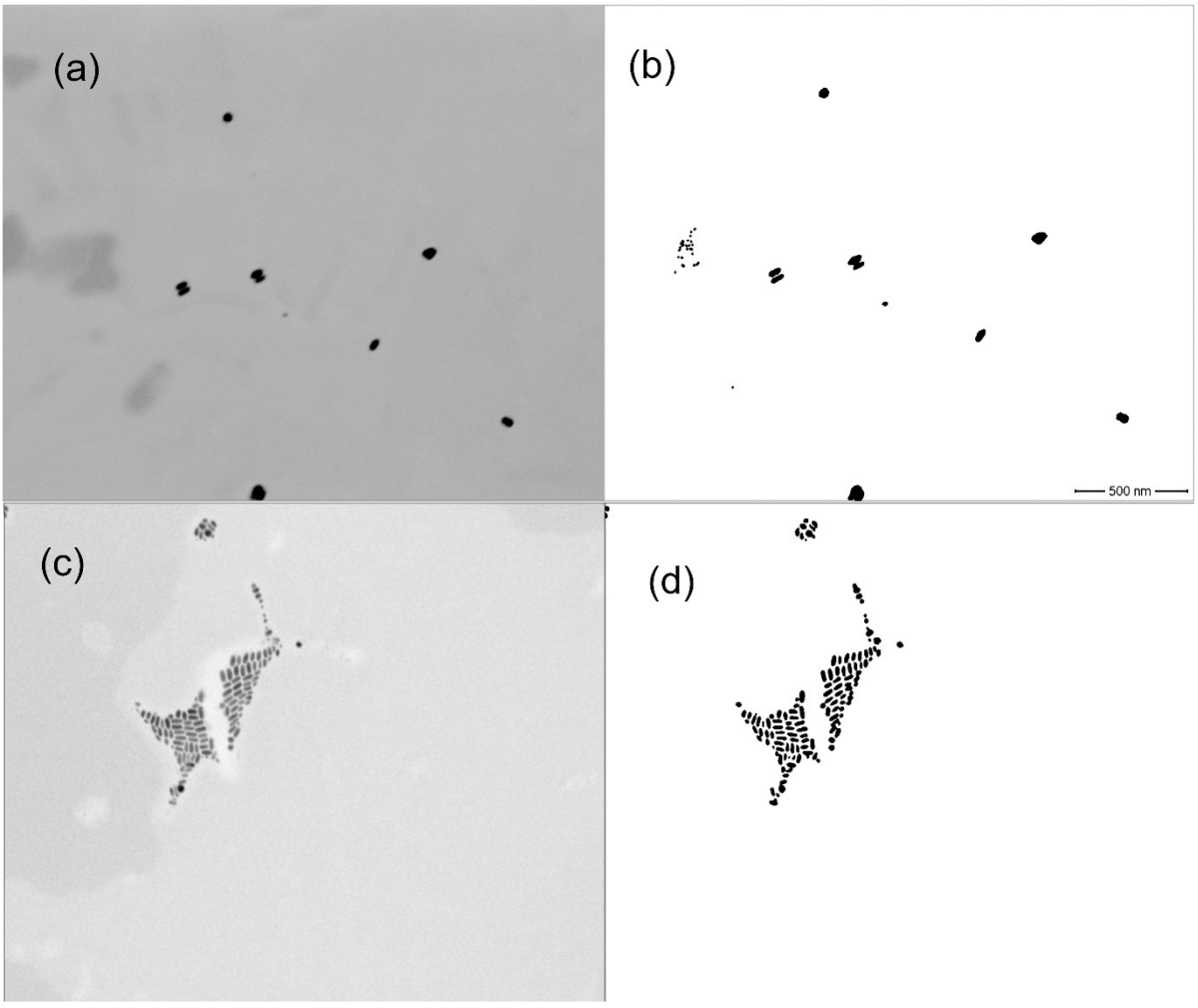

Figure S1. SEM images before (a, c) and after binarization (b, d).

S1.6. Statistical analysis

Through the analysis of the SEM images, we acquired a dataset of particle sizes representing the minor and major axes of the nanorods. In the subsequent step, we computed the aspect ratios of the nanorods for each set after irradiation and fitted the histogram distribution. We adopted a modified lognormal distribution:

$$f(x,\mu^*,\sigma^*) = \frac{A}{x\ln(\sigma^*)\sqrt{2\pi}} exp\left(-\frac{1}{2}\left(\frac{ln(x) - ln(\mu^*)}{ln(\sigma^*)}\right)^2\right), \quad x \in \langle 1,\infty\rangle$$

where A is the normalization factor:

$$A = \frac{2}{1 - erf\left(\frac{-ln(\mu^*)}{ln(\sigma^*)\sqrt{2}}\right)}.$$

In this distribution, x represents an independent variable describing the aspect ratio value, μ^* denotes the median of the distribution, and σ^* represents its dispersion. The modified lognormal distribution is widely used to describe particle size distributions associated with various phenomena, including hail sizes, crystallite radii, and sand particle dimensions [2]. We adapted this distribution by accounting for the fact that the minimal aspect ratio is 1 and not 0 as in an ordinary lognormal distribution. Moreover, the reparameterization of μ^* and σ^* provided a straightforward method of presenting values, as the confidence interval covered by this distribution from μ^*/σ^* to $\mu^* \bullet \sigma^*$ preserves the same properties as the mean and variance in a normal distribution. The distribution was fitted to the data using the maximum likelihood estimation (MLE) method with the L-BFGS-B algorithm. An example of fitting the histogram distribution of the aspect ratios is shown in Fig. 3.

We utilized the Monte Carlo method to estimate uncertainties. We generated 10,000 sets of aspect ratios for each irradiation by simulating from the primary estimates of μ^* and σ^*. Subsequently, we calculated μ^* and σ^* using the MLE method for each set. We then computed the covariance matrix for the primary μ^* and σ^* values across all of our estimates. To ensure the validity of the entire process, we compared the covariance ellipses with the likelihood function contour. The following equation defines the contour of the likelihood function:

$$\sum_i ln\left(f\left(x_i,\mu^*,\sigma^*\right)\right) = \frac{1}{2}$$

The covariance ellipses are consistent with the likelihood contours, as demonstrated in Fig. S2. Hence, our process is valid and adheres to asymptotic behavior. In the final step, we gathered all calculated μ^* and σ^* values and their uncertainties and plotted them as a function of the advancing irradiations. This approach allowed us to describe the modifications in the median and dispersion of the aspect ratio distribution during the irradiation process, as depicted in Fig. 2(e) and 2(f).

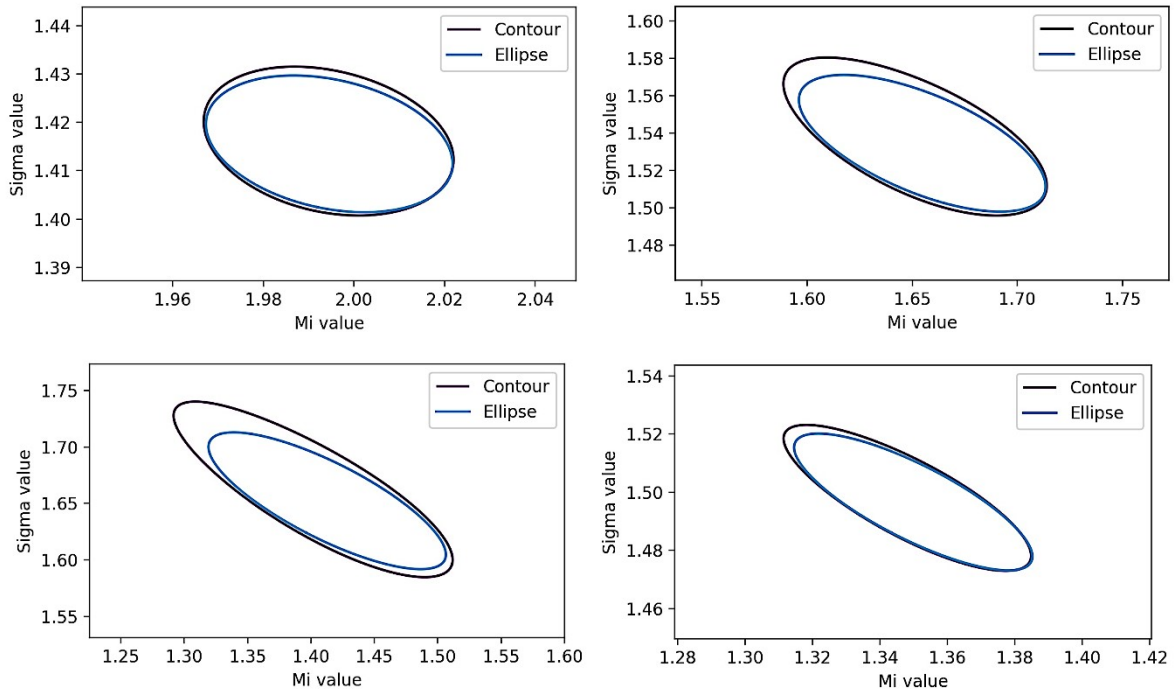

Figure S2. Likelihood contours and covariance ellipses for the fitted distributions for data obtained before (a) and after irradiation steps 4 (b), 8 (c), and 12 (d).

S2. Simulations of extinction spectrum

For the numerical simulations, we approximated the nanorods as prolate ellipsoids, with the *x* dimension elongated with respect to the *y* and *z* dimensions. We also assumed that the *y* and *z* dimensions of our nanorods were equal, which meant that *x* was measured as the major axis, while *y* and *z* were considered the minor axis dimensions. Based on this assumption and the data obtained from the SEM images, we conducted numerical simulations using a modified Maxwell–Garnett formula for randomly oriented prolate ellipsoids, as shown in Ref. [3]:

$$e_{eff} = e_1 + e_1 \frac{\sum_N \sum_{j=x,y,z} \frac{f_j \quad e_m - e_1}{3\,e_1 + L_j(e_m - e_1)}}{1 - \sum_N \sum_{j=x,y,z} \frac{f_i \quad L_j(e_m - e_1)}{3\,e_1 + L_j(e_m - e_1)}}$$

In this formula, e_1 describes the electrical permittivity of the surrounding medium, and e_m is the electrical permittivity of the nanorod. L_j is a geometrical factor value that depends on the electricity of the ellipsoid. f_j is a filling factor. Data for the electrical permittivity of gold and water was collected from the literature [4].

The filling factor can be calculated based on the concentration and average sizes of the minor and major axes. In our case, its value was about 10^{-5}. Therefore, in the simulation, the filling factor was rescaled, and the

average filling factor of the whole set of nanorods was about 10^{-5}. The following formula describes the geometrical factor L with eccentricity e for prolate ellipsoids:

$$L_y = \frac{1-e^2}{e^2}\left(-1+\frac{1}{2e}ln\frac{1+e}{1-e}\right)$$

$$L_y = L_z = \frac{1-L_1}{2}, \quad e^2 = 1-\frac{b^2}{a^2}$$

X, Y, and *Z* are the orthogonal directions of the nanorod, b is the minor axis, and a is the major axis.

In the next step, we converted the electrical permittivity to a complex index of refraction and calculated the absorption spectra from the equation:

$$A = log_{10}(e)\beta z, \quad \beta = \frac{4\pi\kappa}{\lambda}$$

where β is the absorption coefficient of the mixture and κ is the imaginary part of the refractive index of the mixture. In Fig. S3, we present simulated absorption and experimental extinction spectra. The simulated spectra are qualitatively similar and reproduce the positions of the local maxima of bands.

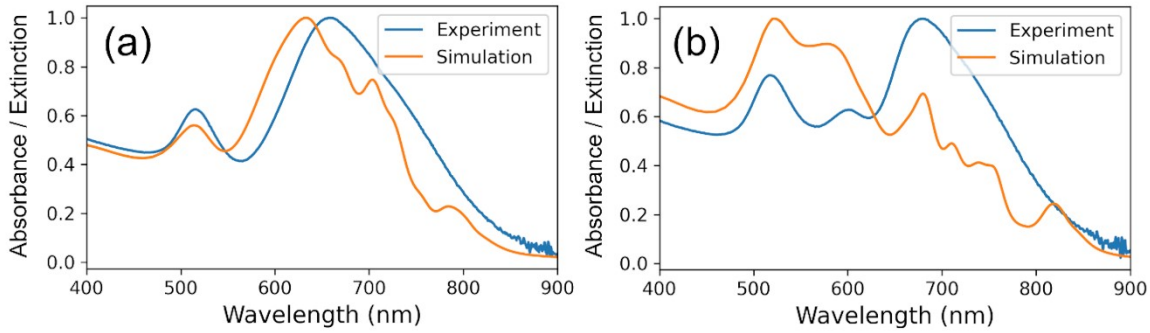

Figure S3. A comparison between the measured and simulated spectra (normalized) before (a) and after (b) the fourth irradiation step (at 620 nm).

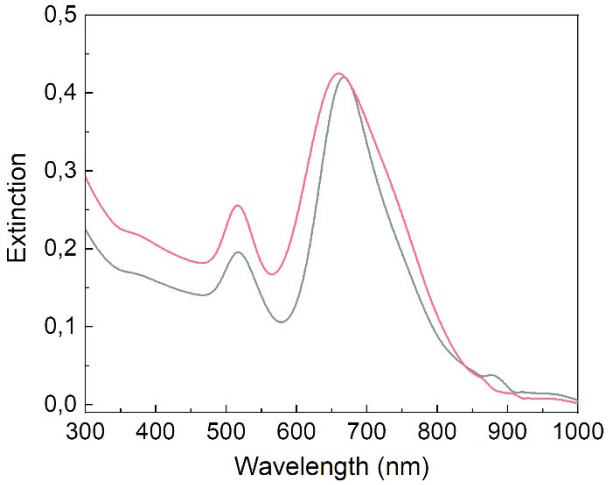

S3. Reproducibility

Figure S4 presents the extinction spectra of two samples of GNR colloid prepared with two consecutive batches using the same chemical procedure, as described in Section S1.2. Due to the various factors influencing the chemical synthesis, such as substrate temperature, stirring rate, and reagent mixing rate, the resulting colloids exhibit slightly different distributions of GNR sizes and are characterized by slightly different extinction spectra.

Figure S4. Extinction spectra of the first (red curve) and second (black curve) GNR colloids before laser irradiation.

The following Figures S5–S8 present the results of the irradiation and analysis of the second batch of GNR colloid.

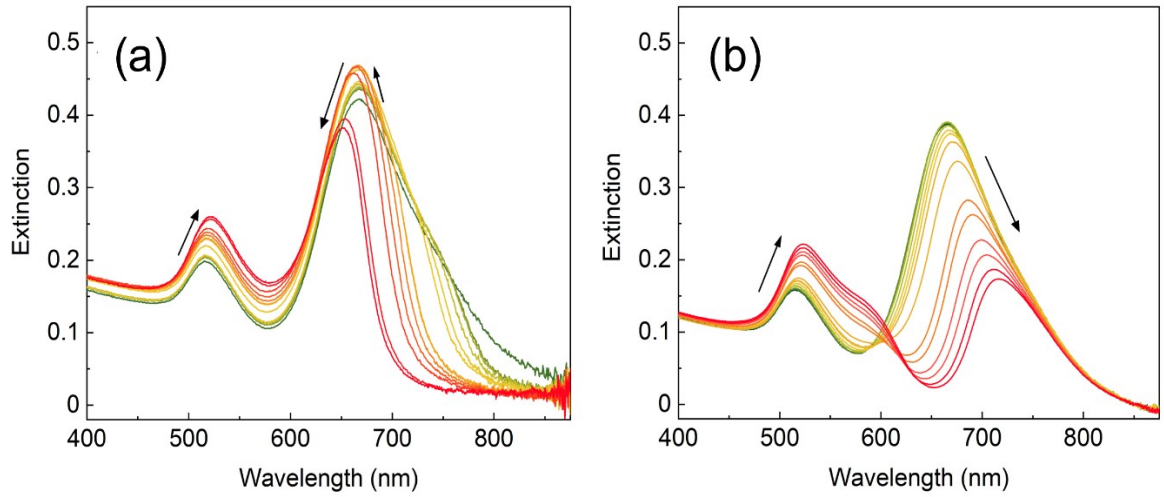

Figure S5. The evolution of the extinction spectra of the second GNR colloid during irradiation on the long- (830−710 nm, a) and short- (580−650 nm, b) wavelength sides of the LSPR band. The consecutive irradiation starts with the green curve and ends with the red curve. The arrows indicate the directions of the changes.

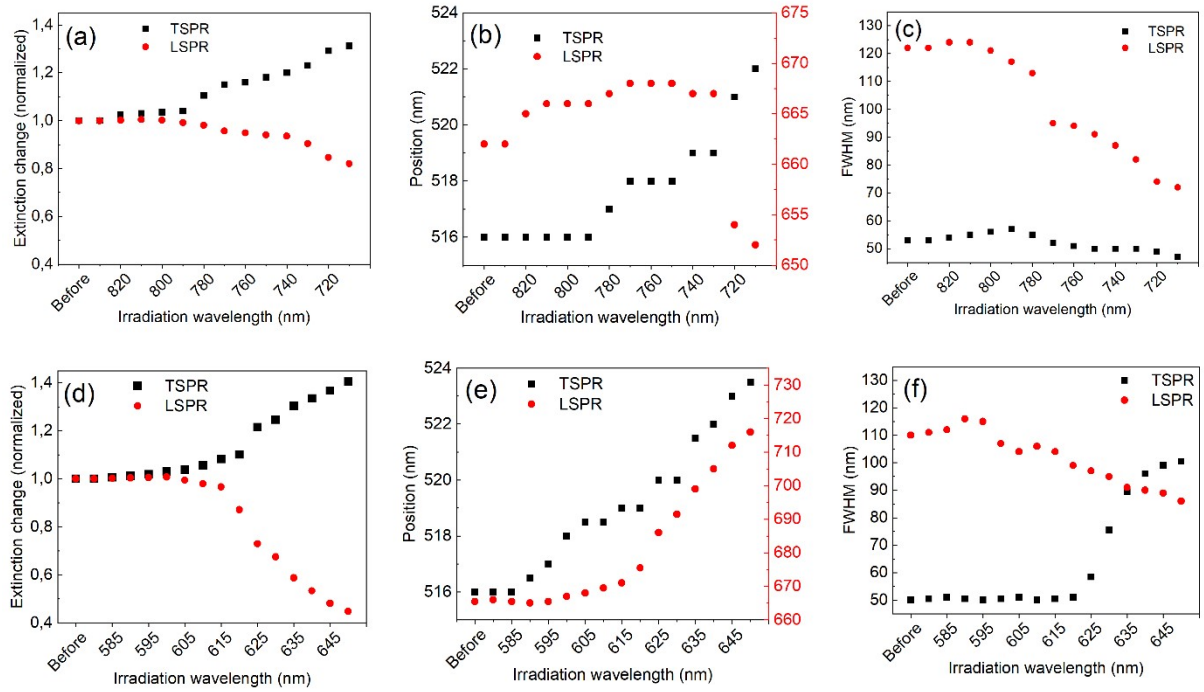

Figure S6. The evolution of specific spectral parameters during the irradiation procedure: extinction (a and d), TSPR positions (b and e), TSPR and LSPR FWHM (c and f), for longer- and shorter-wavelength LSPR band side irradiations, respectively.

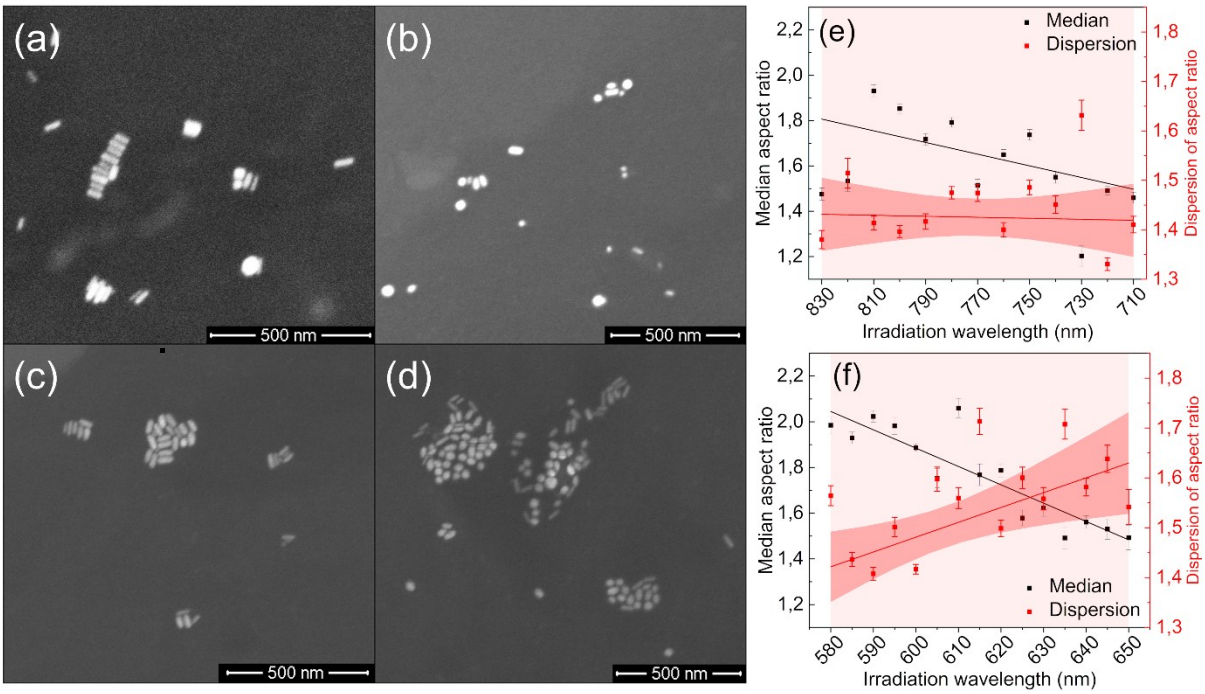

Figure S7. SEM images of GNRs before laser irradiation (a, c) and after irradiation on the longer- (b) and shorter- (d) wavelength sides of the LSPR band. Changes in the median and dispersion of the aspect ratio distribution of GNRs observed after irradiation on the longer- (e) and shorter- (f) wavelength sides of the LSPR band. The red shadows show 95% confidence intervals.

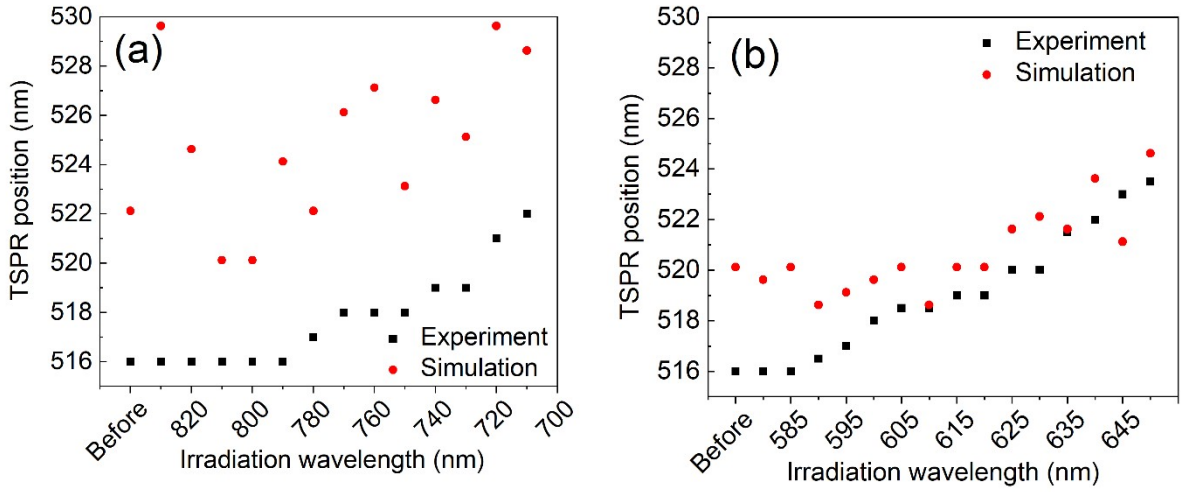

Figure S8. A comparison between simulation and experiment for the maximum wavelength of the TSPR band for the long- (a) and short- (b) wavelength sides of the LSPR band irradiation processes, respectively.

References

1. Nikoobakht, B.; El-Sayed, M. A. Preparation and Growth Mechanism of Gold Nanorods (NRs) Using Seed-Mediated Growth Method. *Chem. Mater.* 2003, **15**, 1957–1962, doi:10.1021/cm020732l.

2. Limpert, E.; Stahel, W. A.; Abbt, M. Log-Normal Distributions across the Sciences: Keys and Clues: On the Charms of Statistics, and How Mechanical Models Resembling Gambling Machines Offer a Link to a Handy Way to Characterize Log-Normal Distributions, Which Can Provide Deeper Insight into Variability and Probability—Normal or Log-Normal: That Is the Question. *BioScience* 2001, **51**, 341–352, doi:10.1641/0006-3568(2001)051[0341:LNDATS]2.0.CO;2.

3. Sihvola, A. Electromagnetic Mixing Formulas and Applications; London, 1999, ISBN 978-0-85296-772-0.

4. Rosenblatt, G.; Simkhovich, B.; Bartal, G.; Orenstein, M. Nonmodal Plasmonics: Controlling the Forced Optical Response of Nanostructures. *Phys. Rev. X* 2020, **10**, 011071, doi:10.1103/PhysRevX.10.011071.